Transfer Function Based Approaches to Array Calibration

Hasan S. Mir
MIT Lincoln Laboratory, Lexington, MA, USA
Email: hmir@mit.edu

***Abstract*— This paper examines transfer-function based techniques for performing direction finding on a source of electromagnetic energy using a passive vector sensor array whose manifold is only nominally known. This problem is studied in the context of a situation in which the source can be observed from multiple look angles, as would be the case for an airborne array. The calibration algorithms examined in this paper address the case of both polarization and non-polarization diverse arrays. Computational studies are presented to assess the efficacy of the calibration algorithms.**

***Index Terms*— array calibration, direction finding, angle of arrival estimation**

I. Introduction

This paper investigates direction finding (DF) on a source of electromagnetic energy using a passive sensor array. The response of a sensor array varies as a function of the direction of the incoming signal. Knowledge of the form of this function, termed the *array manifold* or *array steering vector*, is what enables a sensor array to be used for DF applications.

The specific type of sensor array studied in this paper is the electromagnetic vector sensor, whose usage for direction finding was first proposed in [1]. A conventional (non polarization diverse) sensor array consists of identical sensor element types. A vector sensor is a polarization diverse array whose output is a measurement of multiple components of electromagnetic information. A typical full vector sensor consists of two orthogonal triads of dipole and loop antennas with the same phase center, as shown in Figure 1. The dipoles for measuring the electric field components and the loops measure the magnetic field components.

The utility of a vector sensor can be appreciated by recalling that the angular resolution of an array is inversely related to the size of its aperture. Thus, fine angular resolution will require a larger physical aperture. However, many airborne reconnaissance missions employ small unmanned aerial vehicles on which the physical space available on the airframe is very limited, thus constraining the size of the array aperture. However, because a vector sensor uses multiple components of electromagnetic information, it can offer accurate source location estimates with a smaller aperture. In theory, if a full vector sensor with a point aperture can provide enough sensitivity to measure the complete electric and magnetic fields, the source location can be estimated by simply calculating the Poynting vector.

In practice, the actual (measured) array manifold will differ, often times significantly, from the theoretical (modeled) array manifold. This difference is due various array anomalies such as sensor pattern differences, sensor coupling, and sensor to receiver electrical cable length differences. In order to obtain reliable source direction estimates, DF systems require that a precise characterization of the actual array manifold be available. *Array calibration* is the technique used to relate the actual and theoretical array manifolds. *This paper presents an overview of the array calibration techniques proposed in [2]-[4]*. While most of the available techniques for array calibration are designed for a conventional sensor array [4]-[8], this paper also presents a discussion of the array calibration technique proposed in [2] that explicitly accounts for the polarization diverse nature of the vector sensor (see [3] for an in-depth discussion). The calibration techniques discussed in this paper utilize a transfer-function based framework to relate the modeled and measured steering vectors.

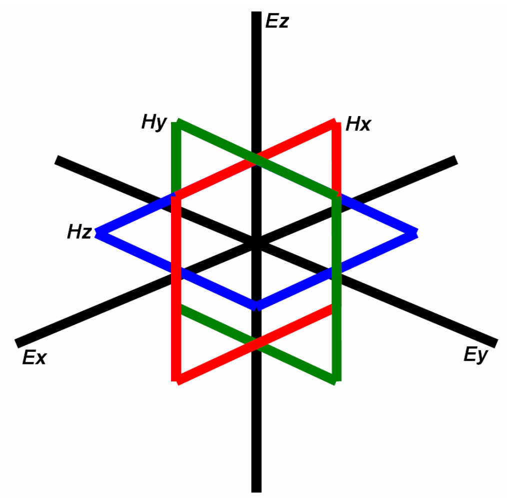

Fig. 1. A full electromagnetic vector sensor.

II. Organization

This paper is organized as follows- Section III develops the steering vector model for a polarization diverse array. Section IV formulates the calibration algorithms. Section

V presents the simulation results and discussion of applying the calibration algorithms developed in Section IV.

III. Steering Vector Model Formulation

Studies such as those in [10] have shown that when the vector sensor in Figure 1 is mounted on a typical small aircraft, some elements of the vector sensor experience significant airframe interaction, resulting in unreliable measurements. To overcome this problem, one solution is to use a "trimmed" vector sensor, whereby only sensor elements with insignificant airframe interaction are retained. By situating multiple trimmed vector sensors at various sites on the airframe, the aperture can be increased. Note that because of aerodynamic issues and/or varying sensor interaction at different locations on the airframe, the trimmed vector sensors will in general not be identical. This concept of distributed and trimmed vector sensors has previously been studied in [11]-[14].

A particular 8-channel trimmed vector sensor configuration that will be studied as an example in this paper is shown in Figure 2. The two loop antennas measure the x and y components of the magnetic field (H_x, H_y), while the vertical dipole measures the z component of the electric field E_z.

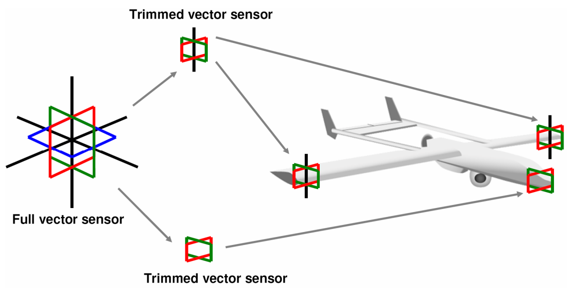

Fig. 2. Trimmed vector sensors and an 8-channel aircraft configuration.

A. Signal Model

Let θ and ϕ represent the azimuth and elevation angle of arrival (AOA), respectively, of the signal on the array with respect to the source location. It is assumed that the vector sensor array is in the far-field of a narrowband signal. Following [15], define the components of the electric and magnetic field received on the array as

$$\begin{bmatrix} E_x \\ E_y \\ E_z \\ H_x \\ H_y \\ H_z \end{bmatrix} = \begin{bmatrix} \cos(\theta)\cos(\phi) & -\sin(\theta) \\ \sin(\theta)\cos(\phi) & \cos(\theta) \\ -\sin(\phi) & 0 \\ -\sin(\theta) & -\cos(\theta)\cos(\phi) \\ \cos(\theta) & -\sin(\theta)\cos(\phi) \\ 0 & \sin(\phi) \end{bmatrix} \begin{bmatrix} \sin(\gamma)\, e^{+j\eta} \\ \cos(\gamma) \end{bmatrix}$$
$$= \mathbf{\Theta}(\theta,\phi)\,\mathbf{p}(\gamma,\eta)$$

where $\mathbf{\Theta}(\theta,\phi)$ and $\mathbf{p}(\gamma,\eta)$ have obvious definitions, and $0^\circ \le \gamma \le 180^\circ$ and $-180^\circ \le \eta \le 180^\circ$ are the polarization angle and phase difference, respectively. Note that while knowledge of γ and η are required to completely characterize the array manifold, only the AOA parameters θ and ϕ are of interest.

Suppose there are N_m sensors of a particular type, and let $\mathbf{R}_m \in \mathbb{R}^{3\times N_m}$ be the corresponding sensor location matrix. Let $\mathbf{\Theta}_m(\theta,\phi)$ be the appropriate row of $\mathbf{\Theta}(\theta,\phi)$ corresponding to the particular field component that the sensors measure. Define a unit vector in the source direction

$$\mathbf{u}(\theta,\phi) = \begin{bmatrix} \cos(\theta)\sin(\phi) & \sin(\theta)\sin(\phi) & \cos(\phi) \end{bmatrix}^T \tag{1}$$

The plane wave (far-field) response is defined as

$$\mathbf{v}_m(\theta,\phi) = e^{+j\frac{2\pi}{\lambda}\mathbf{R}_m^T\mathbf{u}(\theta,\phi)} \tag{2}$$

where λ is the signal wavelength. The response/steering vector of the vector sensor array is generated by concatenating the response of identical sensor types

$$\mathbf{v}_{\mathrm{vs}}(\theta,\phi,\gamma,\eta) = \begin{bmatrix} \mathbf{v}_{\mathrm{vs},1}(\theta,\phi,\gamma,\eta) \\ \vdots \\ \mathbf{v}_{\mathrm{vs},M}(\theta,\phi,\gamma,\eta) \end{bmatrix} \tag{3}$$

where

$$\mathbf{v}_{\mathrm{vs},m}(\theta,\phi,\gamma,\eta) = \mathbf{v}_m(\theta,\phi)\left[\mathbf{\Theta}_m(\theta,\phi)\,\mathbf{p}(\gamma,\eta)\right] \tag{4}$$

and M is the number of distinct field components being measured, or equivalently, the number of different sensor types. The size of the vector $\mathbf{v}_{\mathrm{vs}}(\theta,\phi,\gamma,\eta)$ corresponds to the total number of sensor elements (channels), and will be denoted by N.

As an example, consider the 8-channel trimmed vector sensor configuration shown in Figure 2, which measures the three components H_x, H_y, and E_z. Thus, the value of M equals 3. Letting v_{lw}, v_{rw}, and v_{t} represent the plane wave response for the sensors on the left wing, right wing, and tip of the aircraft, respectively, the trimmed vector sensor response becomes

$$\mathbf{v}_{\mathrm{vs}}(\theta,\phi,\gamma,\eta) = \begin{bmatrix} \begin{pmatrix} v_{\mathrm{lw}} \\ v_{\mathrm{rw}} \end{pmatrix} E_z \\ \begin{pmatrix} v_{\mathrm{lw}} \\ v_{\mathrm{rw}} \\ v_{\mathrm{t}} \end{pmatrix} H_x \\ \begin{pmatrix} v_{\mathrm{lw}} \\ v_{\mathrm{rw}} \\ v_{\mathrm{t}} \end{pmatrix} H_y \end{bmatrix}$$

for which indeed $N = 8$.

Alternative response representations for a polarization diverse array are possible. For example, in certain sensor configurations, it is possible to represent the response as a hypercomplex number (quaternion). This representation is descrbied in more detail in [16],[17].

IV. Array Calibration

Suppose an N element sensor array observes a stationary, far-field, narrowband source at K known and distinct look angles. Let $\mathbf{v}(\theta_k,\phi_k)$ and $\mathbf{z}(\theta_k,\phi_k)$ represent the

$N \times 1$ modeled and measured array steering vector, respectively, for the source azimuth AOA θ_k and elevation AOA ϕ_k, where $k = 1 \ldots K$. The modeled steering vector is constructed based on knowledge of various parameters such as the nominal array geometry and source AOA.

Define

$$\mathbf{V}(\boldsymbol{\theta},\boldsymbol{\phi}) \triangleq \begin{bmatrix} \mathbf{v}(\theta_1,\phi_1) & \ldots & \mathbf{v}(\theta_K,\phi_K) \end{bmatrix}$$

and

$$\mathbf{Z}(\boldsymbol{\theta},\boldsymbol{\phi}) \triangleq \begin{bmatrix} \mathbf{z}(\theta_1,\phi_1) & \ldots & \mathbf{z}(\theta_K,\phi_K) \end{bmatrix}$$

where $\boldsymbol{\theta}$ and $\boldsymbol{\phi}$ are vectors whose kth elements are θ_k and ϕ_k, respectively.

In order to perform array calibration, a transfer-function operator $\mathbf{T}\{\}$ is sought such that when it operates on the modeled steering vector, the result is a "good" approximation of the measured steering vector. That is,

$$\mathbf{z}(\theta_k,\phi_k) \approx \mathbf{T}\{\mathbf{v}(\theta_k,\phi_k)\} \tag{5}$$

To quantify the notion of a "good" fit, the Euclidean distance between the left and right hand side of (5) will be minimized, resulting in the cost function

$$J = \sum_{k=1}^{K} \left\|\mathbf{z}(\theta_k,\phi_k) - \mathbf{T}\{\mathbf{v}(\theta_k,\phi_k)\}\right\|^2 \tag{6}$$

(6) can be recast as

$$J = \left\|\mathbf{Z}(\boldsymbol{\theta},\boldsymbol{\phi}) - \mathbf{T}\{\mathbf{V}(\boldsymbol{\theta},\boldsymbol{\phi})\}\right\|_F^2 \tag{7}$$

In [4],[5], the following form of $\mathbf{T}\{\}$ was considered:

$$\mathbf{T}\{\mathbf{v}(\theta_k,\phi_k)\} \quad = \quad \mathbf{A}\mathbf{v}(\theta_k,\phi_k) \tag{8}$$

where $\mathbf{A} \in \mathbb{C}^{N\times N}$ is a calibration matrix. Substituting (8) into (7) and differentiating yields the optimal solution for $\mathbf{A}$:

$$\mathbf{A} = \mathbf{Z}(\boldsymbol{\theta},\boldsymbol{\phi})\,\mathbf{V}^{\#}(\boldsymbol{\theta},\boldsymbol{\phi}) \tag{9}$$

where $^{\#}$ denotes the matrix pseudo-inverse. Because the calibration matrix minimizes the distance between the measured and modeled steering vectors, it is useful in DF applications where the modeled steering vector is used to determine the source AOA. Note that (9) was developed for a conventional array and does not assume polarization diversity. In [4], it was shown that (9) yields significant performance improvement when used with a conventional array. It is reasonable to expect that some performance gain will also be achieved when (9) is used on a polarization diverse array. However, further performance improvement when using a polarization diverse array may be possible if the transfer-function in (8) is extended to explicitly account for the polarization diversity. Towards this end, the following observation due to [9] is made: Let two distinct signal polarization vectors be denoted by

$$\mathbf{p}_1 \quad = \quad \mathbf{p}(\gamma_1,\eta_1) \tag{10}$$

$$\mathbf{p}_2 \quad = \quad \mathbf{p}(\gamma_2,\eta_2) \tag{11}$$

Denote their respective vector sensor steering vectors as $\mathbf{v}_{\rm vs}(\theta,\phi,\mathbf{p}_1)$ and $\mathbf{v}_{\rm vs}(\theta,\phi,\mathbf{p}_2)$. The steering vector for an arbitrary polarization $\mathbf{p}$ at look angle k may be expressed as

$$\mathbf{v}_{\rm vs}(\theta_k,\phi_k,\mathbf{p}) = c_{1k}\mathbf{v}_{\rm vs}(\theta_k,\phi_k,\mathbf{p}_1) + c_{2k}\mathbf{v}_{\rm vs}(\theta_k,\phi_k,\mathbf{p}_2) \tag{12}$$

where $c_{1k}, c_{2k} \in \mathbb{C}$. Thus, the polarization state is parameterized by a 2-dimensional subspace, and c_{1k} and c_{2k} represent the linear combination coefficients needed to achieve a particular polarization state.

(12) can be expanded in terms of $\mathbf{v}(\theta_k,\phi_k)$ as

$$\begin{aligned}\mathbf{v}_{\rm vs}(\theta_k,\phi_k,\mathbf{p}) = {} & c_{1k}\boldsymbol{\Gamma}_1(\theta_k,\phi_k,\mathbf{p}_1)\,\mathbf{v}(\theta_k,\phi_k) \\ & + c_{2k}\boldsymbol{\Gamma}_2(\theta_k,\phi_k,\mathbf{p}_2)\,\mathbf{v}(\theta_k,\phi_k)\end{aligned} \tag{13}$$

where $\boldsymbol{\Gamma}_1(\theta_k,\phi_k,\mathbf{p}_1) \in \mathbb{C}^{N\times N}$ and $\boldsymbol{\Gamma}_2(\theta_k,\phi_k,\mathbf{p}_2) \in \mathbb{C}^{N\times N}$ are diagonal matrices consisting of terms of the form $\boldsymbol{\Theta}_m(\theta_k,\phi_k)\,\mathbf{p}(\gamma,\eta)$. When the array manifold is perturbed from the modeled array manifold, as is the case in realistic scenarios, (13) can be extended so that the angle-dependent terms in $\boldsymbol{\Gamma}_1(\theta_k,\phi_k,\mathbf{p}_1)$ and $\boldsymbol{\Gamma}_2(\theta_k,\phi_k,\mathbf{p}_2)$ as well as the remaining manifold perturbations, are captured in the corresponding full matrices $\mathbf{A}_1 \in \mathbb{C}^{N\times N}$ and $\mathbf{A}_2 \in \mathbb{C}^{N\times N}$, so that

$$\mathbf{T}\{\mathbf{v}\} = c_{1k}\mathbf{A}_1\mathbf{v}(\theta_k,\phi_k) + c_{2k}\mathbf{A}_2\mathbf{v}(\theta_k,\phi_k) \tag{14}$$

where $\{c_{1k}, c_{2k}, \mathbf{A}_1, \mathbf{A}_2\}$ are the unknown calibration parameters.

The corresponding cost function in the form of (7) is

$$J_{PD} \triangleq \left\|\mathbf{Z}(\boldsymbol{\theta},\boldsymbol{\phi}) - \mathbf{A}_D\left[\mathbf{P}\odot\left(\vec{\mathbf{1}}_2\otimes\mathbf{V}(\boldsymbol{\theta},\boldsymbol{\phi})\right)\right]\right\|_F^2 \tag{15}$$

where $\otimes$ denotes the Kronecker tensor product, $\odot$ denotes the element-by-element Hadamard product [20] and

$$\mathbf{A}_D \triangleq \begin{bmatrix} \mathbf{A}_1 & \mathbf{A}_2 \end{bmatrix} \tag{16}$$

$$\mathbf{P} = \begin{bmatrix} \vec{\mathbf{1}}_N \otimes \begin{bmatrix} c_{11} & \ldots & c_{1K} \end{bmatrix} \\ \vec{\mathbf{1}}_N \otimes \begin{bmatrix} c_{21} & \ldots & c_{2K} \end{bmatrix} \end{bmatrix} \tag{17}$$

Differentiating (15) yields the optimal solution for the calibration matrices

$$\mathbf{A}_D = \mathbf{Z}(\boldsymbol{\theta},\boldsymbol{\phi})\left[\mathbf{P}\odot\left(\vec{\mathbf{1}}_2\otimes\mathbf{V}(\boldsymbol{\theta},\boldsymbol{\phi})\right)\right]^{\#} \tag{18}$$

Note that (18) assumes knowledge of the coefficients c_{1k} and c_{2k}, which have not yet been computed. To solve for these coefficients, observe that since it is desired that $\mathbf{T}\{\mathbf{v}(\theta_k,\phi_k)\} = \mathbf{z}(\theta_k,\phi_k)$, (14) can be rewritten as

$$\begin{bmatrix} \mathbf{A}_1\mathbf{v}(\theta_k,\phi_k) & \mathbf{A}_2\mathbf{v}(\theta_k,\phi_k) \end{bmatrix} \begin{bmatrix} c_{1k} \\ c_{2k} \end{bmatrix} = \mathbf{z}(\theta_k,\phi_k) \tag{19}$$

The least squares solution for c_{1k} and c_{2k} as such is

$$\mathbf{c}_k \triangleq \begin{bmatrix} c_{1k} \\ c_{2k} \end{bmatrix} = \begin{bmatrix} \mathbf{A}_1\mathbf{v}(\theta_k,\phi_k) & \mathbf{A}_2\mathbf{v}(\theta_k,\phi_k) \end{bmatrix}^{\#}\mathbf{z}(\theta_k,\phi_k) \tag{20}$$

The optimization of the calibration parameters can now be performed by iterating between (18) and (20). The optimization may be initialized by selecting $\mathbf{A}_D^{(0)} = [\mathbf{Z}(\boldsymbol{\theta},\boldsymbol{\phi})\,\mathbf{V}^{\#}(\boldsymbol{\theta},\boldsymbol{\phi}) \quad \mathbf{I}_N]$, where the superscript represents the iteration number. Convergence is achieved for a tolerance level δ when $\left\|\mathbf{A}_D^{(i)} - \mathbf{A}_D^{(i-1)}\right\|_F / N^2 < \delta$, where $\|(\cdot)\|_F$ denotes the Frobenius norm [20].

A. Usage in Direction Finding Algorithms

The form of (14) suggests that its usage in a direction finding algorithm would require a search over c_{1k} and c_{2k} as well as θ_k and ϕ_k, thereby doubling the dimensionality of the search space. However, consider a direction finding estimator of the form

$$F\left(\theta_k,\phi_k,c_{1k},c_{2k}\right) = \frac{\left\|\mathbf{M}^H\left(c_{1k}\mathbf{A}_1\mathbf{v}\left(\theta_k,\phi_k\right)+c_{2k}\mathbf{A}_2\mathbf{v}\left(\theta_k,\phi_k\right)\right)\right\|^2}{\left\|c_{1k}\mathbf{A}_1\mathbf{v}\left(\theta_k,\phi_k\right)+c_{2k}\mathbf{A}_2\mathbf{v}\left(\theta_k,\phi_k\right)\right\|^2} \quad (21)$$

Then $\arg\min_{\theta_k,\phi_k,c_{1k},c_{2k}} F(\theta_k,\phi_k,c_{1k},c_{2k})$ when $\mathbf{M}$ is the matrix of eigenvectors corresponding to the noise subspace of the received signal is the MuSIC estimator [21]. When (21) is rewritten with the aid of (19) as

$$F\left(\theta_k,\phi_k,c_{1k},c_{2k}\right) = \frac{\left\|\mathbf{M}^H\left(\left[\begin{array}{cc}\mathbf{A}_1\mathbf{v}\left(\theta_k,\phi_k\right) & \mathbf{A}_2\mathbf{v}\left(\theta_k,\phi_k\right)\end{array}\right]\mathbf{c}_k\right)\right\|^2}{\left\|\left[\begin{array}{cc}\mathbf{A}_1\mathbf{v}\left(\theta_k,\phi_k\right) & \mathbf{A}_2\mathbf{v}\left(\theta_k,\phi_k\right)\end{array}\right]\mathbf{c}_k\right\|^2} \quad (22)$$

it is recognized as a Rayleigh quotient, and the solution for $\mathbf{c}_k$ is thus the extremal eigenvector of the matrix

$$\mathbf{Q}\mathbf{Q}^H$$

where

$$\mathbf{Q} = \left[\begin{array}{cc}\mathbf{A}_1\mathbf{v}\left(\theta_k,\phi_k\right) & \mathbf{A}_2\mathbf{v}\left(\theta_k,\phi_k\right)\end{array}\right]^H\mathbf{M} \quad (23)$$

Hence, the existence of an analytical solution for $\mathbf{c}_k$ leaves the dimensionality of the search space unchanged.

B. Synthetic Elements

Recall that because of airframe interaction, some elements of the full vector sensor were removed, resulting in a "trimmed" vector sensor. The elements that were removed can be viewed as lost degrees of freedom. The introduction of synthetic or "virtual" sensor elements may help recapture some of the source localization performance that is lost due to element trimming. Consider an N element sensor array and the corresponding N element modeled steering vector. Now suppose that an additional N_{syn} sensor elements are included in the modeled steering vector, even if they do not exist physically. The modeled steering vector now consists of the original N element steering vector concatenated with an N_{syn} element vector whose elements are the modeled sensor response at the locations of the synthetic elements. The calibration cost function may now be posed as

$$J = \sum_{k=1}^{K}\left\|\mathbf{z}\left(\theta_k,\phi_k\right) - \mathbf{T}\left\{\left[\begin{array}{c}\mathbf{V}\left(\boldsymbol{\theta},\boldsymbol{\phi}\right)\\ \mathbf{V}_{syn}\left(\boldsymbol{\theta},\boldsymbol{\phi}\right)\end{array}\right]\right\}\right\|^2 \quad (24)$$

Note that the optimization for the calibration matrices is now over $\mathbb{C}^{N\times(N+N_{syn})}$.

The specific placement of synthetic elements is generally performed in an ad-hoc manner. For example, for arrays with a regular geometry, synthetic elements can be placed via concentric extension. For arrays in which certain elements are "missing" (as is the case with the trimmed vector sensor), a natural choice is to position the synthetic elements at the locations of the missing elements.

Synthetic elements provide additional fitting coefficients (N_{syn} additional coefficients per array element) for the calibration process, resulting in superior calibration performance, though at the cost of added computational complexity.

V. Simulation Results

A. Simulation Setup

The trimmed vector sensor configuration in Figure 2 is used for simulation studies. The aircraft geometry at 90 MHz is shown in Figure 3.

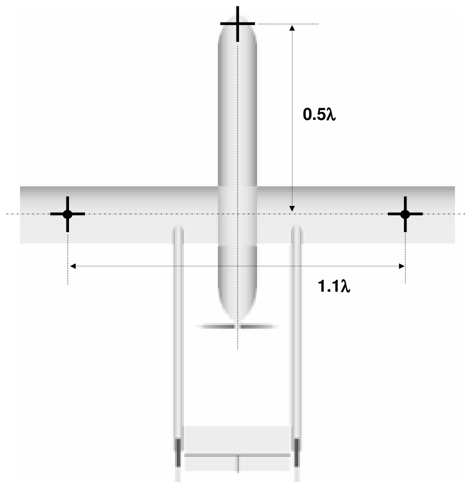

Fig. 3. Small aircraft geometry at 90 MHz with 3 trimmed vector sensor sites (c.f. Figure 2).

Sensor manifold perturbations are assumed to be caused by near-field scatterers local to the airframe. For every look angle k, the measured steering vector $\mathbf{z}(\theta_k,\phi_k)$ is modeled as follows:

$$\begin{aligned}\mathbf{z}\left(\theta_k,\phi_k\right) &= \mathbf{v}_{\mathrm{vs}}\left(\theta_k,\phi_k\right)\\ &+ \varepsilon\sum_{s=1}^{N_{\mathrm{scat}}}\left[\begin{array}{c}\mathbf{v}_1\left(\theta_s,\phi_s\right)\left[\boldsymbol{\Theta}_1\left(\theta_s,\phi_s\right)\boldsymbol{\Gamma}_s\mathbf{p}\left(\gamma,\eta\right)\right]e^{+jd_s}\\ \vdots\\ \mathbf{v}_M\left(\theta_s,\phi_s\right)\left[\boldsymbol{\Theta}_M\left(\theta_s,\phi_s\right)\boldsymbol{\Gamma}_s\mathbf{p}\left(\gamma,\eta\right)\right]e^{+jd_s}\end{array}\right]\end{aligned} \quad (25)$$

The model (25) consists of the direct path steering vector $\mathbf{v}_{\mathrm{vs}}(\theta_k,\phi_k)$, and the multipath component which is modeled by the summation terms. The relative strength of the multipath component is controlled by the parameter ε, and N_{scat} denotes the number of scatterers. For simulation purposes, $\varepsilon = 10$ dB and $N_{\mathrm{scat}} = 20$. Observe that the term $\mathbf{v}_m\left(\theta_s,\phi_s\right)\left[\boldsymbol{\Theta}_m\left(\theta_s,\phi_s\right)\boldsymbol{\Gamma}_s\mathbf{p}\left(\gamma,\eta\right)\right]$ in (25) is identical to (4), except that the polarization state vector $\mathbf{p}(\gamma,\eta)$ is premultiplied by $\boldsymbol{\Gamma}_s$. The 2×2 matrix $\boldsymbol{\Gamma}_s$ is a random scattering matrix which models the scatterer-induced transformation of polarization state. d_s is the path length difference which causes a phase offset modeled by the term e^{+jd_s}.

TABLE I
PERFORMANCE OF CALIBRATION ALGORITHMS.

Algorithm	$\bar{\varepsilon}_\theta$ **(Deg)**	$\bar{\varepsilon}_\phi$ **(Deg)**
Initial Estimate	3.01	2.98
No Calibration	12.05	16.27
Conventional Calibration	0.77	0.40
Conventional Calibration w/Synth Elem	0.04	0.03
Pol Div Calibration	0.13	0.05
Pol Div Calibration w/Synth Elem	0.005	0.007

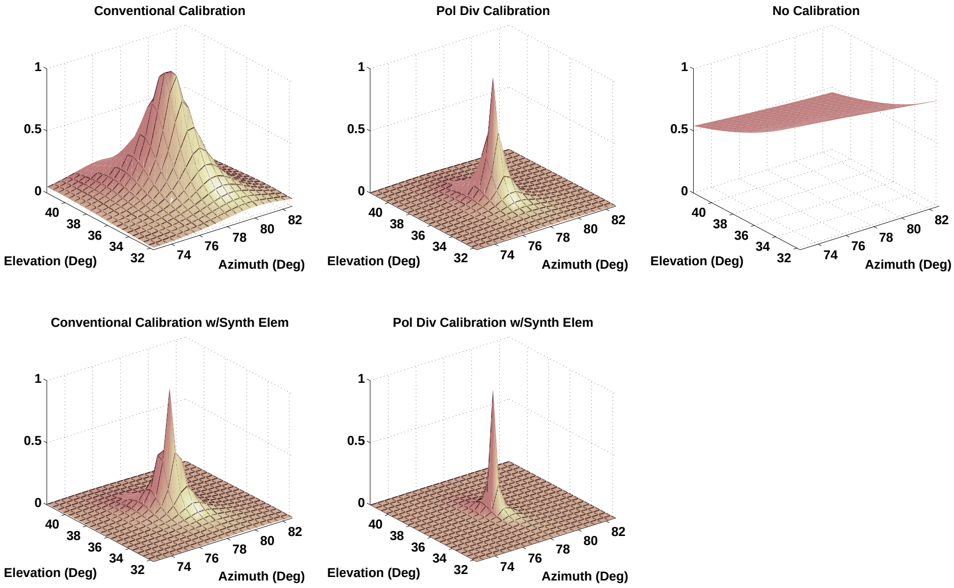

Fig. 4. Example DF spectra for various calibration algorithms.

For the study presented in this paper, simulations were performed using 200 calibration points randomly sampled over the set of data taken in $90°$ azimuth and $30°$ elevation sectors. The presented results are the average of 10 trials.

For comparison purposes, direction finding performance is evaluated without the usage calibration, and with usage of conventional array calibration (9) and polarization diverse array calibration (18). The performance improvement using synthetic elements is also presented. In this paper, synthetic elements are chosen as the full vector sensor elements (Figure 1) missing from the trimmed vector sensors. As such, because a full vector sensor consists of 6 elements, the 8-channel configuration of Figure 2, which consists of 3 distinct subarrays, would have a modeled steering vector of length 18 when synthetic elements are used.

The root mean square error (RMSE) of the AOA estimation error is the metric used for performance assessment, and is defined as the RMSE of the difference between the elements in the estimated and actual AOAs, so that

$$\bar{\varepsilon}_\theta = \sqrt{\frac{1}{K}\sum_{k=1}^{K}\left(\hat{\theta}_k - \theta_k\right)^2} \quad (26)$$

and

$$\bar{\varepsilon}_\phi = \sqrt{\frac{1}{K}\sum_{k=1}^{K}\left(\hat{\phi}_k - \phi_k\right)^2} \quad (27)$$

for azimuth and elevation errors, respectively.

B. Discussion

Figure 4 makes apparent that the use of calibration significantly helps in reducing the width of the DF spectral peak, as compared to the no calibration scenario in which the peak is very spread out. It is evident that use of polarization diverse calibration offers a significant performance advantage over the use of conventional calibration. Table I offers a quantitative algorithm performance comparison. From an initial guess error of a few degrees, not performing calibration will significantly worsen performance. This is because uncalibrated array perturbations can cause a measured steering vector from a particular look angle to closely match a modeled steering vector that originates from a very different look angle. However after performing calibration, the AOA RMSE is reduced to a fraction of a degree. While the results presented in this paper use simulated, rather than experimental data, and may thus be somewhat optimistic, the simulation results do nonetheless show that a significant performance gain over conventional array calibration algorithms is possible when a polarization diverse array is calibrated using an algorithm that explicitly accounts for the polarization diversity.

VI. Conclusion

A review of transfer-function based approaches to array calibration was presented. Two approaches- one for a conventional (non-polarization diverse) array and one for a polarization diverse array, were examined. Both are based on a least squares metric and as such lend themselves to efficient solutions. Simulation studies for a trimmed and distributed polarization diverse array were carried out. While the benefits of calibration are evident with usage of the conventional array calibration approach, a marked performance improvement was seen with usage of the polarization diverse calibration approach. Performance enhancement was also seen for both calibration approaches when synthetic elements were used.

References

[1] A. Nehorai and E. Paldi, "Vector-Sensor Array Processing for Electromagnetic Source Localization," *IEEE Trans. Sig. Proc.*, vol. 42, pp. 376-398, Feb. 1994.

[2] H. Mir and J. Sahr, "Calibration of a Polarization Diverse Array," *2006 Inter Conf on Acous. Speech. and Sig Proc*, pp. 1065-1068 , May 2006.

[3] H. Mir. and J. Sahr, "Passive Direction Finding Using Airborne Vector Sensors in the Presence of Manifold Perturbations ," *IEEE Trans. Sig. Proc.*, vol. 55, pp. 156-164, Jan. 2007.

[4] H. Mir. et al, "Self-Calibration of an Airborne Array," *38th Asilomar Conf. Sig., Sys. Comp.*, pp. 2340-2344 , Nov. 2004.

[5] J. Pierre and M. Kaveh, "Experimental performance of calibration and direction-finding algorithms," *ICASSP-91*, pp. 1365-1368, May 1991.

[6] A. Flieller et. al., "Robust Bearing Estimation In the Presence of Direction-Dependent Modelling Errors: Identifiability and Treatment," *ICASSP-95*, pp. 1884-1887, May 1995.

[7] T. Ratnarajah and A. Manikas, "An H_∞ Approach To Mitigate the Effects of Array Uncertainties On the MUSIC Algorithm," *IEEE Sig. Proc. Let.*, vol. 5, pp. 185-188, Jul. 1998.

[8] G.H. Whipple, C.M. Keller, and K.W Forsythe, "Performance Characterization of External Array Self Calibration Algorithms Using Experimental Data," *34th Asilomar Conf. Sig., Sys. Comp.*, pp. 623-628, Oct. 2000.

[9] E. Ferrara and T. Parks, "Direction Finding with an Array of Antennas Having Diverse Polarizations," *IEEE Trans. Ant. & Prop.*, vol. 31, pp. 231 - 236, Mar. 1983.

[10] D. Bliss, A. Chan, and A. Eapen, "Vector Sensor Array Design," MIT Lincoln Laboratoy Presentation, April 13, 2004.

[11] K. T. Wong and M. D. Zoltowski, "Self-Initiating MUSIC Direction Finding and Polarization Estimation in Spatio-Polarizational Beamspace," *IEEE Trans. Ant. & Prop.*, vol. 48, pp. 1235-1245, August 2000.

[12] K. T. Wong, "Direction Finding / Polarization Estimation — Dipole and/or Loop Triad(s)," *IEEE Trans. Aerospace & Electronic Sys.*, vol. 37, pp. 679-684, April 2001.

[13] K. T. Wong, L. Li and M. D. Zoltowski, "Root-MUSIC-Based Direction-Finding and Polarization-Estimation Using Diversely-Polarized Possibly-Collocated Antennas," *IEEE Ant. Wireless Prop. Letters*, vol. 3, pp. 129-132, 2004.

[14] K. T. Wong and A. K.-Y. Lai, "Inexpensive Upgrade of Base-Station Dumb-Antennas by Two Magnetic Loops for Blind Adaptive Downlink Beamforming, *IEEE Antennas & Propagation Magazine*, vol. 47, pp. 189-193, February 2005.

[15] K.T. Wong and M.D. Zoltowski, "Closed-form Direction Finding and Polarization Estimation With Arbitrarily Spaced Electromagnetic Vector-sensors at Unknown Locations," *IEEE Trans. Ant. & Prop.*, vol. 48, pp. 671 - 681, May 2000.

[16] S. Miron, N. Bihan, and J.I Mars, "High Resolution Vector-Sensor Array Processing Based on Bi-Quaternions ," *2006 Inter Conf on Acous. Speech. and Sig Proc*, pp. 1077-1080 , May 2006.

[17] S. Miron, N. Bihan, and J.I Mars, "Quaternion-MUSIC for vector-sensor array processing ," *IEEE Trans. Sig. Proc.*, vol. 54, pp. 1218-1229, Apr. 2006.

[18] W. Stutzman and G. Thiele, *Antenna Theory and Design*, Wiley, 1997.

[19] L. Trefethen and D. Bau, *Numerical Linear Algebra*, SIAM, 1997.

[20] T. Moon and W. Stirling, *Mathematical Methods and Algorithms for Signal Processing*, Prentice Hall, 200.

[21] R.O. Schmidt, "Multiple Emitter Location and Signal Parameter Estimation," *IEEE Trans. Ant. & Prop.*, vol. 34, pp. 276-280, Mar. 1986.

[22] J.A. Nelder and R. Mead, "A Simplex Method for Function Minimization" *Computer Journal*, vol. 7, pp. 308-313, 1965.

[23] R. Fletcher, *Practical Methods of Optimization*, John Wiley & Sons, 1980.

[24] W. H. Press, B. P. Flannery, S. A. Teukolsky, and W. T. Vettering, *Numerical Recipes in C*, Cambridge University Press, 1988.

[25] S. Haykin, *Adaptive Filter Theory*, Prentice Hall, 1996.

[26] D. Manolakis, V. Ingle, and S. Kogon, *Statistical and Adaptive Signal Processing: Spectral Estimation, Signal Modeling, Adaptive Filtering and Array Processing*, McGraw-Hill, 2000.

[27] H. Van Trees, *Optimum Array Processing (Detection, Estimation, and Modulation Theory, Part IV)*, Wiley-Interscience, 2002.

Hasan Mir was born on June 27, 1982. He received the B.S. (cum laude), M.S., and Ph.D. degrees in electrical engineering from the University of Washington, Seattle, in 2000, 2001, and 2005 respectively. He was the recipient of the MIT Lincoln Laboratory Ph.D. fellowship. Currently, he is a member of the Air Defense Techniques group at MIT Lincoln Laboratory. His research interests are in array signal processing.